Journal of Materials Science: Materials in Electronics
https://doi.org/10.1007/s10854-017-8453-6

Chemical spray pyrolysis synthesis of covellite copper sulphide (CuS) thin films for economical counter electrode for DSSCs

Kiran Diwate[1] · Sachin Rondia[1] · Azam Mayabadi[1] · Avinash Rokade[1] · Ravindra Waykar[1] · Haribhau Borate[1] · Adinath Funde[1] · Manish Shinde[2] · M. B. Rajedra Prasad[3] · Habib Pathan[3] · Sandesh Jadkar[3]

Received: 21 October 2017 / Accepted: 18 December 2017

Abstract
Thin films of covellite copper sulphide (CuS) were deposited on FTO substrates using chemical spray pyrolysis technique. Influence of Cu-to-S molar ratio on structural, surface morphological, optical and electrical properties were systematically investigated using variety of characterization techniques. Formation of covellite CuS films was confirmed by low angle-XRD and Raman spectroscopy. The field emission scanning electron microscopy analysis revealed the formation of faceted CuS particles without secondary growth. Optical studies exhibited decrease in optical band gap (from 2.21 to 1.69 eV) with increase in Cu-to-S molar ratio. Electrical properties were investigated using Van der Pauw four point probe method and Hall measurements revealed that as-synthesized CuS films have low sheet resistance (1.47–2.45 Ω/□), high carrier mobility (8.90–54.89 cm^2/Vs) and high sheet concentration (10^{16}–10^{18}/cm^2). The CuS films deposited at optimized Cu-to-S molar ratio (1:2.5) were then further studied for electrochemical impedance spectroscopy and photovoltaic characteristics. A quantum-dot sensitized solar cell incorporating optimized CuS film as counter electrode showed power conversion efficiency of ~ 1.05% with V_{oc} ~ 0.46 V, I_{sc} ~ 1.01 mA/cm^2 and fill factor ~ 0.34%. Although the cell is not fully optimized and better results can be anticipated.

1 Introduction

In recent years, there has been an increasing interest in transition metal chalcogenides due to their novel physical and chemical properties. Among them copper sulphide (Cu_xS) is considered as a promising material for solar energy conversation system, due to their structural and electrical properties [1]. It is well-known that Cu_xS possesses seven stable crystal modifications (with x = 2, 1.96, 1.8, 1.75, 1.32, 1.12, and 1) [2]. Out of the seven existing copper sulfides phases with different stoichiometries, only five known to be stable at room temperature. These are CuS (covellite), $Cu_{1.75}S$ (anilite), $Cu_{1.8}S$ (digenite), $Cu_{1.96}S$ (djurleite) and Cu_2S (chalcocite) [3]. This allows the properties of Cu_xS to be tuned in a broad range. In particular, the band gap of Cu_xS has values from 1.2 eV for the copper-rich phase Cu_2S to 2 eV for copper deficient CuS [4]. Due to unique physical properties such as superionic conductivity [5] superconductivity [6] or p-type conductivity [7] the copper sulfide (Cu_xS) has been successfully used in photo thermal conversion [8], solar cells [9], electrodes [10], nonlinear optical materials, solar controller, solar radiation absorber [11], catalyst [12], nanometer scale switches [13] and high-capacity cathode material in lithium secondary batteries [14], sensors [15], plasmonic applications [16] etc. Recently, CuS nanostructures in various forms and shapes have been reported for different applications which proved that growing interest of researchers in this material [17–22].

For the deposition of CuS thin films various techniques have been used which includes sputtering [23], electrodeposition [24], co-evaporation [25], organic deposition [26], atomic layer deposition [3], vacuum evaporation [27], chemical vapour deposition (CVD) [28], dip coating [29], wet chemical route [30], chemical bath deposition (CBD) [31] and chemical spray pyrolysis deposition [32], successive ionic layer absorption and reaction (SILAR) [33], sol–gel [34] etc. Each deposition method has its own advantages and

✉ Sandesh Jadkar
sandesh@physics.unipune.ac.in

1 School of Energy Studies, Savitribai Phule Pune University, Ganeshkhind Road, Pune 411 007, India

2 Centre for Materials for Electronics Technology (C-MET), Pashan Road, Pune 411 007, India

3 Department of Physics, Savitribai Phule Pune University, Ganeshkhind Road, Pune 411 007, India

Published online: 26 December 2017

limitations. Among these, chemical spray pyrolysis method has many advantages over the others such as its simplicity, cost effectiveness, possibility of large area deposition, minimum material wastage and no need to deal with poisonous gases and no requirement of costly sophisticated instruments. Furthermore, properties of CuS thin films can be controlled easily by varying various process parameters such as flow rate, deposition time, concentration and pH of spraying solution, type of substrate etc. However, capabilities of chemical spray pyrolysis for obtaining device quality CuS have not been fully established. It has been observed that variation in molar concentration of the copper and chalcogen precursor plays an important role in determining the structural, morphological, optical and electrical properties of the fabricated CuS thin films and only few reports exist in the literature [35, 36]. With this motivation an attempt has been made to investigate the effect of Cu-to-S molar ratio on properties of CuS thin films by chemical spray pyrolysis method.

In the present work, we report synthesis of CuS films on FTO substrate by chemical spray pyrolysis method at various Cu-to-S molar ratios in the precursor solution. The structural, surface morphological, optical and electrical properties of as-synthesized CuS films have been studied using low angle-XRD, Raman spectroscopy, field emission scanning electron microscopy (FE-SEM), UV–Visible spectroscopy and four probe resistivity and Hall Effect measurements. Cyclic voltammetry (CV) and electrochemical impedance spectroscopy (EIS) analysis have been also carried out on optimized CuS layer in view of its use as counter electrode in DSSCs. Finally, photovoltaic characteristics of DSSC with employment of optimized CuS counter electrode are also presented.

2 Experimental

2.1 Cleaning of fluorine doped tin oxide (FTO)

The cleaning of substrates plays an important role in the process of depositions of thin films. In present work, fluorine doped tin oxide (FTO) were used for the depositions of CuS films. The FTO coated glass substrates initially rinsed with double distilled water (DDW). Then substrates were kept in ethanol for 5 min and then again rinsed with double distilled water (DDW). Afterwards it was ultrasonicated in acetone, ethanol and DDW respectively, each for 15 min. Finally, they are dried using nitrogen gas and subjected immediately for deposition of different films.

2.2 Preparation of CuS films

All the chemicals used were of analytical grade (AR) as obtained from Sigma-Aldrich (99% purity). All the chemicals were used as received. The deposition was carried out in an *in-house* built chemical spray pyrolysis (CSP) deposition system. The precursor solution for CuS films was prepared by dissolving copper(II) chloride and thiourea in different Cu:S molar ratios of 1:2.5, 1:3, 1:3.5, 1:4, 1:5 in solution mixture of Water:Ethanol:Glycerol in 7:2:1 volume ratio under constant magnetic stirring at 250 rpm. This solution was spray deposited on cleaned FTO substrates. The substrate temperature was maintained at 325 °C. The air flow rate and nozzle-to-substrate distance were kept constant during the deposition at 22 liters per minute and 28 cm, respectively. The deposition was carried out for 10 min and samples were allowed to cool to room temperature in the CSP system and then taken out for further characterization. Figure 1 depicts the process flow of preparation of Cu_xS films by CSP method. In spray pyrolysis process the growth of CuS films is a result of

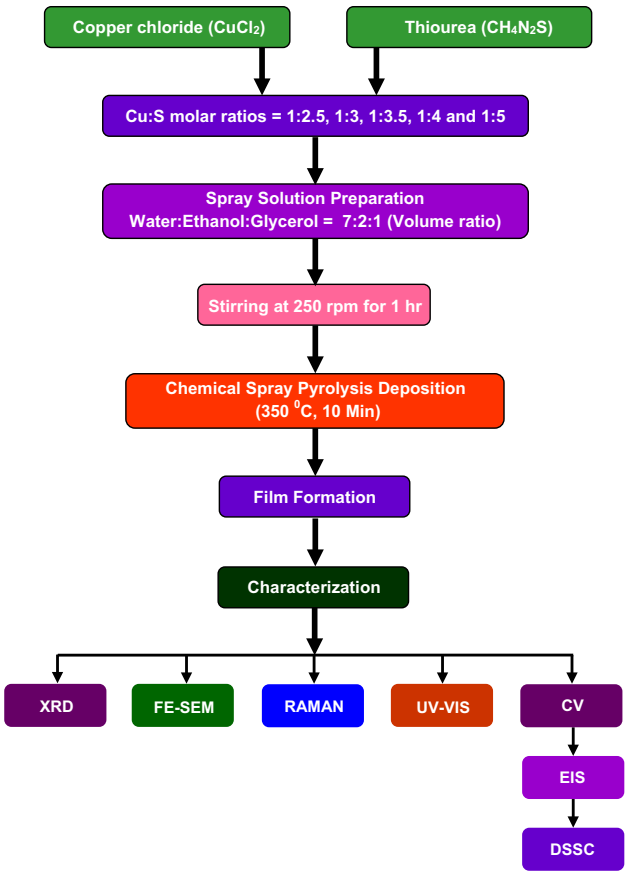

Fig. 1 The process flow for preparation of CuS thin films on FTO and subsequent fabrication of DSSC

several processes taking place on the heated substrate [37]. Hydrolysis of thiourea takes place followed by its reaction with copper ions as the solution droplets approach the substrate which is maintained at higher temperature. The solvent evaporation, nucleation and growth of CuS take place at the substrate leading to formation of crystalline CuS thin film.

2.3 Characterization of CuS films

Low angle X-ray diffraction patterns were obtained by X-ray diffractometer (Bruker D8 Advance, Germany) using Cu K_α line ($\lambda = 1.54056$ Å). The patterns were taken at a grazing angle of 1°. The average crystallite size was estimated using the classical Scherrer's formula. The surface morphology of the films is investigated using field emission scanning electron microscopy (FESEM, Hitachi, S-4800, Japan). The optical properties of CuS films were deduced from transmittance and reflectance spectra of the films deposited on FTO and were measured using a JASCO, V-670 UV–Visible spectrophotometer in the range 250–1100 nm. Raman spectra were recorded using Raman spectrophotometer (Jobin Yvon Horibra, LABRAM-HR) in the range 100–1000 cm^{-1}. The excitation source was 532 nm line of He–Ne laser. Four probe measurements were done to determine the electrical properties of the films using JANDEL model RM3. The type of conductivity and carrier's mobility of CuS films were determined by Hall Effect measurement using HMS3000 at 0.54 T.

2.4 DSSC fabrication and testing

Electrochemical impedance spectroscopy (EIS) measurements were carried out using potentiostat/galvanostat (Ivium Soft:Vertex, The Netherlands) in a typical three-electrode configuration, with the FTO film as working electrode (WE), CuS on FTO as counter electrode (CE), Ag/AgCl as reference electrode (RE). Based on EIS data, the cell showing the best performance was chose for further fabrication of complete DSSC assembly. DSSC was fabricated according to our previous work [38]. In short, thick film prepared by commercial TiO_2 powder was used as photoanode which was sensitized using CdS QDs using successive ionic layer adsorption and reaction (SILAR) method. Sandwich solar cells were fabricated using CdS sensitized TiO_2 as photoanodes and light sensitive materials with CuS as the counter electrode and polysulfide as the electrolyte. J–V characteristics of the cell was studied to evaluate their photovoltaic performance by keeping the cell area ~ 0.25 cm^2 using Kiethley source meter (2420) under illumination of 15 mW with a white LED source.

3 Results and discussion

3.1 Low angle X-ray diffraction analysis

Low angle X-ray diffraction (low angle-XRD) is a widely used nondestructive technique for the structural characterization of different materials. Figure 2 shows XRD pattern of as-deposited CuS films deposited on FTO substrate at various Cu-to-S molar ratios. For comparison, the XRD pattern of FTO substrate (JCPDS card # 41-1445) is also included in Fig. 2. Presence of multiple peaks indicates that as deposited CuS thin films are polycrystalline. As seen from the XRD pattern diffraction peaks are observed at 2θ ~ 27.1°, 27.7°, 29.3°, 31.8°, 32.8°, 38.8°, 52.7° and 59.4° corresponding to (100), (101), (102), (103), (006), (110), (108) and (116) diffraction planes, respectively with preferred orientation along (102) direction. These peak positions were perfectly matched with JCPDS data card # 06-0464 corresponding to the standard XRD pattern of covellite hexagonal phase of CuS. Raman spectroscopy analysis further supports this (discussed later). No other diffraction peaks, except those of the FTO substrate, can be seen suggesting that no other

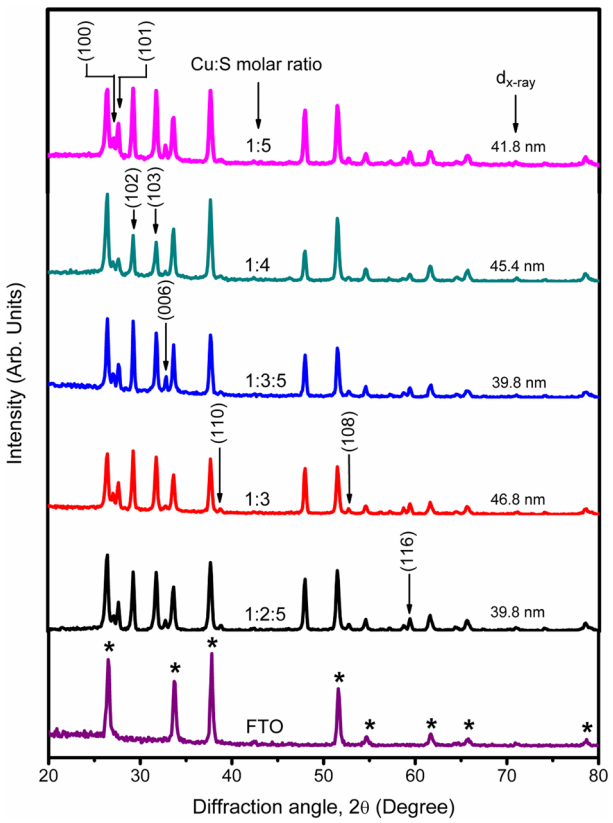

Fig. 2 Low angle X-ray diffraction pattern of CuS films prepared at different Cu-to-S molar ratios on FTO substrate. Asterisk represents indicates diffraction peaks which belong to the FTO substrate

crystalline compounds are found in as-deposited CuS films. Similar results have been reported by Riyaz et al. [34] for CuS nanoparticles prepared by sol–gel method and Saranya et al. [39] by hydrothermal route.

The average grain size was estimated using the classical Scherrer's formula [40],

$$d_{\mathrm{X-ray}} = \frac{0.9\ \lambda}{\beta\ \cos\ \theta_B} \tag{1}$$

where λ is the wavelength of diffracted radiation, θ_B is the Bragg angle and β is the line width (FWHM) in radians and its value was found to be in the range 39–46 nm over the entire range of Cu-to-S molar ratios studied. These values are shown in Fig. 2.

3.2 Raman spectroscopy analysis

Phase composition of different materials including CuS can be effectively determined by Raman spectroscopy. According to the group theory, 2A1g, 2E1g, and 4E2g are the eight Raman active phonon modes for CuS. Figure 3 show Raman spectra of CuS thin films deposited at various Cu-to-S molar ratios. A very intense phonon mode at ~ 475 cm^{-1} which is assigned to vibrational modes from the covalent S–S bonds in crystalline CuS [41] and 3 weak bands ~ 141, 262, and 927 cm^{-1} were observed in the Raman spectra of CuS films. These bands agree well with the reported Raman spectra of covellite CuS [42]. These results are consistent with low angle XRD analysis and further confirm the formation of covellite CuS thin films. A weaker band at ~ 262 cm^{-1} can be assigned to bending and lattice vibrational modes of Cu–S bonding [43]. Presence of another weaker band ~ 927 cm^{-1} is due to the 1st overtone of the band centered ~ 475 cm^{-1}. No other vibrational modes have been observed over the entire range of Cu-to-S molar ratios studied signifying presence of pure CuS phase in the films.

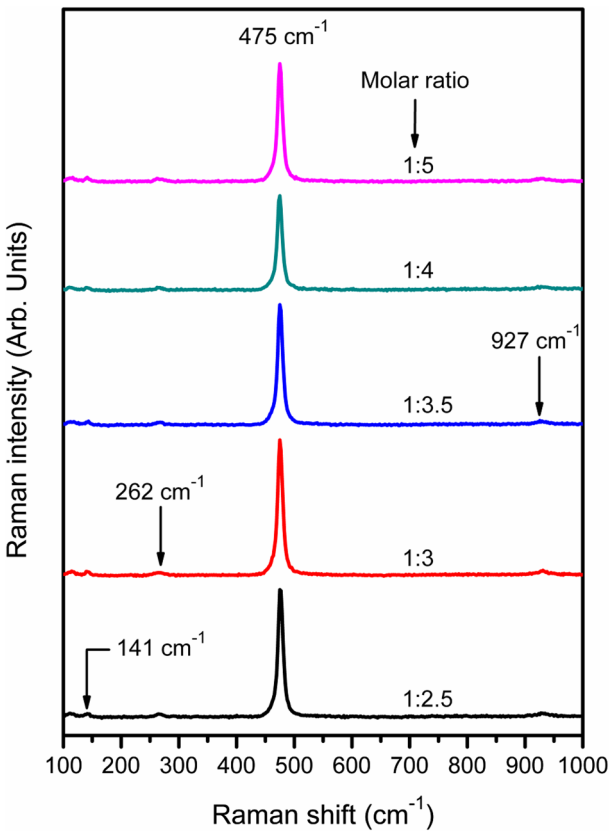

Fig. 3 Raman spectra of CuS thin films prepared at different Cu-to-S molar ratios on FTO substrates

3.3 Surface morphology analysis

To know about the surface morphology of spray pyrolysis deposited CuS thin films FE-SEM analysis were carried out. Figure 4 shows FE-SEM images of CuS thin films at for three different Cu-to-S molar ratios viz; 1:2.5, 1:3.5 and 1:5. All the prepared CuS thin films show uniform surface morphology of faceted growth of particles over the entire FTO substrate.

In case of CuS films deposited at Cu-to-S molar ratio of 1:2.5 (Fig. 4a) show the irregular shaped particles constituting the films without shape edges having more surface roughness. However, for the film grown with Cu-to-S molar ratio of 1:3.5 (Fig. 4b), the particles appear with rectangular brick like shapes having sharp edges. The thickness and length of these particles was found in the range ~ 100–200 nm and ~ 300 nm–1.1 µm, respectively. The CuS films grown at 1:5 molar ratio of Cu and S precursors (Fig. 4c) a dense film made up of irregular particles having thickness ~ 200–400 nm and length of ~ 400 nm–1 µm were observed. These particles have rather blunt edges. One noteworthy feature of films prepared on FTO substrates is that no secondary growth of the particles has been observed.

3.4 UV–Visible spectroscopy analysis

Optical properties of CuS thin films were investigated using UV–Visible spectroscopy. Optical absorption spectra of polycrystalline CuS deposited on FTO substrate recorded in wavelength range 200–1100 nm is shown in Fig. 5a. From the figure it is clear that CuS thin films have high absorbance of light in the visible region of the solar spectrum. In addition, a broad band extending into the near-IR region can be observed, which is characteristic for covellite CuS [34]. There is a broad shoulder ~ 620 nm, in loger wavelength region and near IR region is due to free-carrier absorption and is slightly blue-shifted due to quantum confinement effect of CuS nanomaterial [44] as compared to the bulk CuS material [45]. Low angle XRD

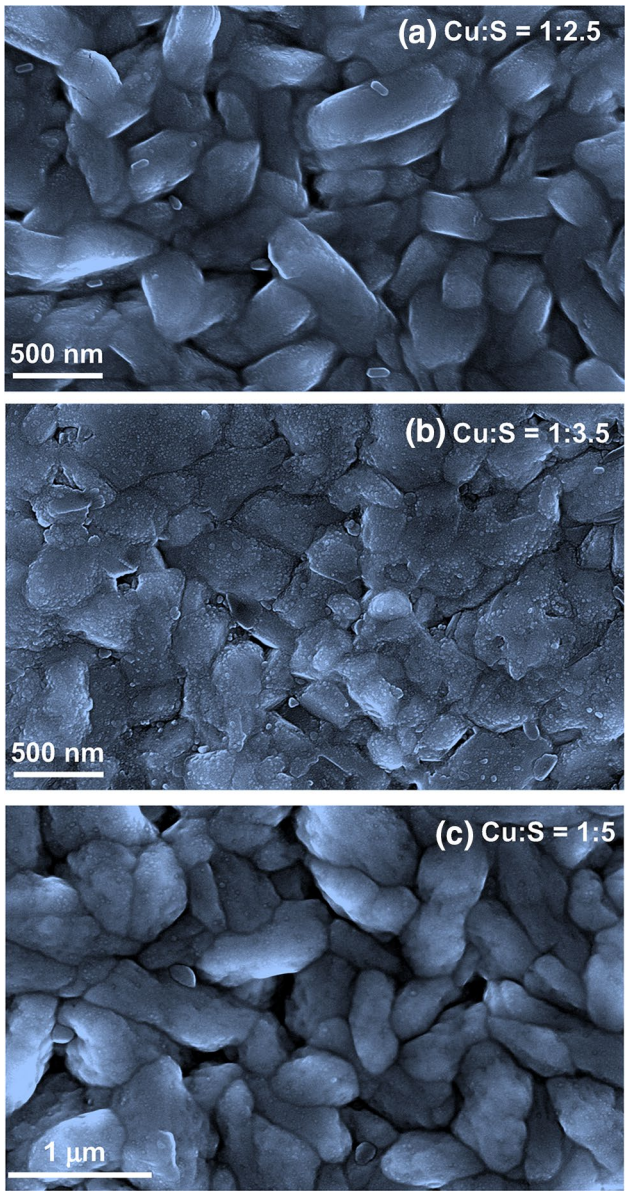

Fig. 4 FE-SEM images of CuS films prepared at **a** 1:2.5, **b** 1:3.5 and **c** 1:5 molar ratios on FTO substrates

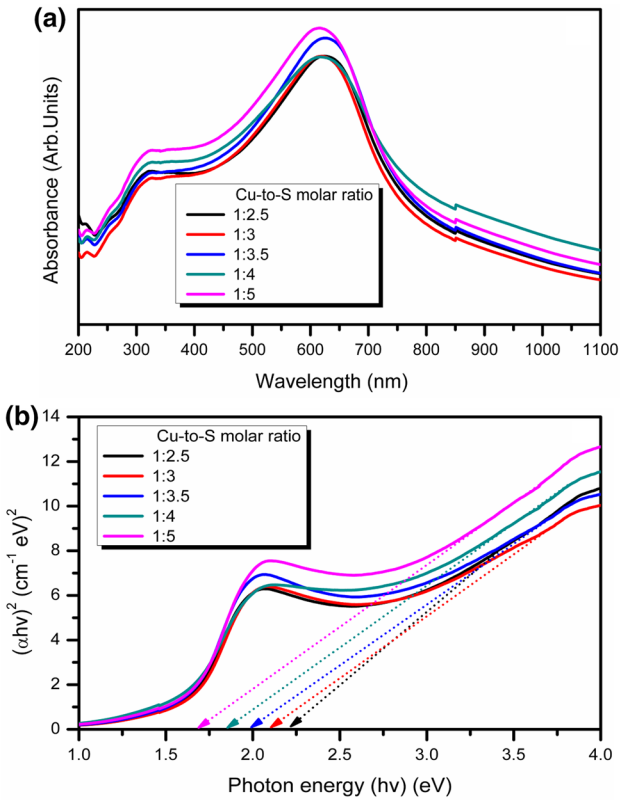

Fig. 5 UV–Visible spectroscopy analysis of CuS films prepared at different Cu-to-S molar ratios on FTO substrates **a** absorption spectra, **b** Tauc plots

analysis support this conjecture. The presence of broad absorption spectrum in both visible and near-IR regions suggest that the CuS is a promising material in the field of photocatalysis and solar cells [46].

In the direct transition semiconductor, the optical energy band gap (E_{opt}) and the optical absorption coefficient (α) are related by [47],

$$(\alpha E)^{1/2} = B^{1/2}(E - E_{opt}) \quad (2)$$

where α is the absorption coefficient, B is the optical density of state and E is the photon energy. The absorption coefficient (α) can be calculated from the transmittance of the films with the formula,

$$\alpha = \frac{1}{d}\ln\left(\frac{1}{T}\right) \quad (3)$$

where d is the thickness of the films and T is the transmittance. Therefore, the optical band gap is obtained by extrapolating the tangential line to the photon energy ($E = h\upsilon$) axis in the plot of $(\alpha h\upsilon)^2$ as a function of $h\upsilon$ (Tauc plot). The optical band gaps of the films was determined from the extrapolation of the linear plot of $(\alpha h\upsilon)^{1/2}$ versus $h\upsilon$ at $\alpha = 0$ (see Fig. 5b). The band gap values of spray pyrolysis deposited CuS thin films for 1:2.5, 1:3, 1:3.5, 1:4, 1:5 Cu-to-S molar ratios are found 2.21, 2.11, 1.99, 1.85 and 1.69 eV respectively. It decreases with increase in Cu-to-S molar ratios. Interestingly, these values are higher than the band gap of bulk CuS (1.2 eV) [48]. It is known that the optical properties of semiconductor nanoparticles depands on their crystallite size and crystallites shape [49]. We attribute decrease in band gap of CuS films to change in average grain size and its shape with increase in Cu-to-S molar ratios. The change in average grain size as reavled by XRD analysis

(Fig. 2) and change in its shape as reavled from FE-SEM analysis (Fig. 4) further support this.

3.5 Electrical properties

The effect of change of electrical properties due to change in Cu-to-S molar ratio of CuS films were studied by four probe resistivity and Hall effect measurements. Four probe measurements were carried out using four probe apparatus (Jandel, Model RM3) at room temperature. The electrical properties of CuS films were obtained by using Hall Effect measurement set-up (ECOPIA HMS-3000) at current of (I) = 1 mA and applied magnetic field of (H) = 0.54 T. Table 1 shows electrical properties of CuS films measured using four probe resistivity measurement and Hall Effect measurement. As seen the CuS films deposited at various Cu-to-S molar ratios have very low sheet resistance in the range of 1.47–2.45 Ω/□. The carrier mobility and sheet concentration were found in the range of 8.90–54.89 cm^2/Vs and 10^{16}–10^{18}/cm^2 respectively. These mobility values are in accordance with the reported values (7.24 cm^2/Vs) by Yuan et al. [50]. The negative value of current observed in Hot Probe experiment [51] and positive sign of average Hall coefficient (not shown) indicates that the CuS thin films deposited at different Cu-to-S molar ratios has p-type conductivity. These results match well with the reports available in the literature [50, 52] and can be attributable to free holes from acceptor levels of copper vacancies [53]. The change in the sheet resistance can be due to the combined effect of change mobility and carrier concentration whereas the change in mobility can be correlated to change in particle size and edge sharpness as observed in FE-SEM analysis.

3.6 Cyclic voltametry (CV) studies

The electro-catalytic activity of CuS thin films deposited on FTO substrate was analyzed using cyclic voltammetry (CV) and is shown in Fig. 6. Cyclic voltammetry is conducted at a scan speed of 100 mV/s and in the voltage range from − 1 to 1 V using polysulphide as electrolyte. The prepared CuS samples are independently used as the counter electrode (CE) and Ag/AgCl as the reference electrode (RE).

Table 1 Electrical properties of CuS films measured using four probe resistivity measurement and hall effect measurement

Four probe measurement			
Cu-to-S molar ratio	1:2.5	1:3.5	1:5
Sheet resistance (Ω/□)	1.47	2.45	2.24
Hall measurements			
Mobility (cm^2/Vs)	8.90	54.89	12.49
Sheet-concentration (/cm^2)	4.19×10^{17}	6.58×10^{16}	2.76×10^{17}

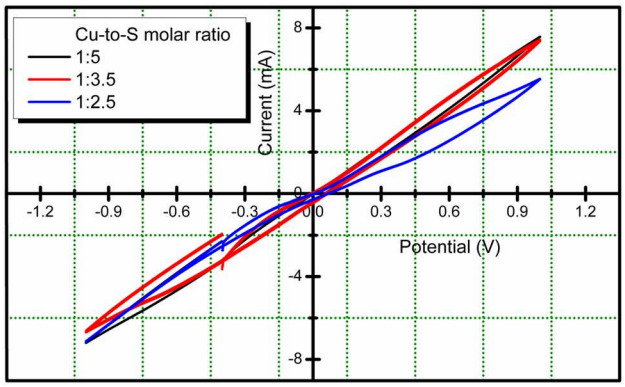

Fig. 6 Cyclic voltammograms of CuS thin films deposited at three Cu-to-S molar ratios, 1:2.5, 1:3.5 and 1:5

The counter electrode prepared from Cu-to-S molar ratio of 1:2.5 shows maximum current density compared to the other two counter electrodes prepared at Cu-to-S molar ratios of 1:3.5 and 1:5. The higher redox activity in counter electrode prepared at 1:2.5 Cu-to-S molar ratio may be due to conversion of oxidized polysulfide S_x^{2-} into S^{2-} on counter electrode surface during the regeneration of cell compared to other two counter electrodes which results higher current density [54]. The lowest sheet resistance observed for CuS film deposited at Cu-to-S molar ratio 1:2.5 further supports this. Hence, CuS film prepared at 1:2.5 Cu-to-S molar ratio has been consider for further investigations.

3.7 Electrochemical impedance spectroscopy (EIS) analysis

The Nyquist diagram of electrochemical impedance spectroscopy (EIS) data is an effective way to measure the electron transfer resistance. The size of the arc radius on the Nyquist plot is directly related to resistance of electron transfer in dye sensitized solar cells (DSSCs). It also reflects the

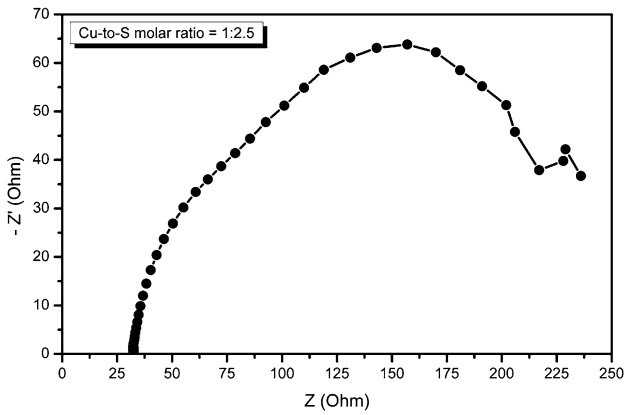

Fig. 7 Nyquist plot for optimized CuS counter electrode

energy barrier of electrode reaction [55]. Figure 7 shows EIS measurements using the Nyquist plots which have been used to analyze the internal resistance of DSSCs [56]. The EIS was carried out in dark in the frequency range between 10 kHz–10 Hz at a bias of −0.7 V and signal amplitude of 10 mV and 0.1 M polysulfide electrolyte by employing Potentiostat/Galvanostat (Ivium Soft:Vertex) electrochemical work station. The arc at high frequency represents the counter electrode/electrolyte interface and the middle arc at intermediate frequency range is attributed to photo electrode/electrolyte interface. The last arc at lower frequency region represents the diffusion of electrolyte species in the electrolyte. The diameter of the first arc quantitatively represents the charge transfer resistance of at counter electrode/electrolyte interface which is of the order of few tens of ohms as it can be seen from the Nyquists plot in the Fig. 7. This value is much lower than the that of Pt when used as counter electrode (few kΩ) and are in compliance with reported results [54, 57].

3.8 Photovoltaic characteristics

Figure 8 presents the J–V characteristics of CdS based DSSC incorporating CuS/FTO counter electrode prepared at 1:2.5 Cu-to-S molar ratio. The inset shows the schematic of CdS based DSSC used in the present study. The active area of the photovoltaic device is 0.25 cm^2. A 15 mW white LED light was used for the illumination. The J–V curve which indicates the solar cell performance with the x-intercept of the curve representing the open circuit voltage and the y-intercept gives the short circuit current density. The open circuit voltage was obtained to be ~0.46 V while the short circuit current density was 1.01 mA/cm^2. The fill factor was ~0.34% and a solar cell power conversion efficiency of ~1.05% has been obtained. Similar results were also obtained by other researchers [17]. Although the obtained power conversion efficiency is very low, the present study is just a beginning and has laid the foundation for further studies towards the use of cost effective thin film counter electrode material in DSSCs. As the cell is not fully optimized and better results can be anticipated.

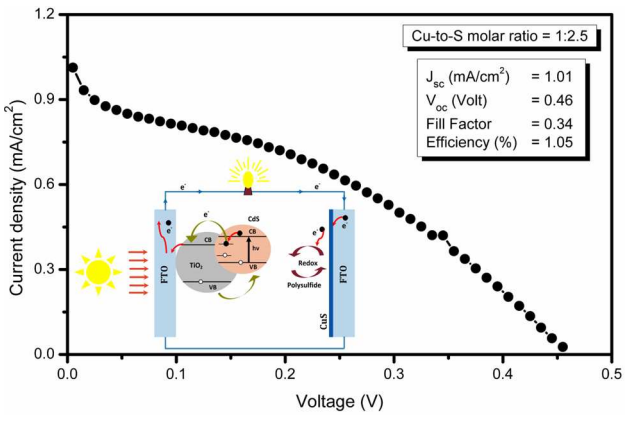

Fig. 8 J–V characteristics of DSSC incorporating optimized CuS counter electrode. The inset shows schematic of typical DSSC used with CuS counter electrode

4 Conclusions

In the present study, thin films of covellite copper sulphide (CuS) were deposited on FTO substrates using chemical spray pyrolysis technique at various Cu-to-S molar ratios. Structural, morphology, optical, electrical and electrochemical properties of these films have been systematically investigated using variety of characterization techniques such as low angle-XRD, Raman spectroscopy, UV–Visible spectroscopy, FE-SEM, Van der Pauw four point probe method, Hall measurements, cyclic voltammetry (CV), electrochemical impedance spectroscopy (EIS) etc. Formation of covellite CuS films has been confirmed by low angle-XRD and Raman spectroscopy. The surface morphology analysis revealed the formation of faceted CuS particles without secondary growth with increase in Cu-to-S molar ratio. Optical studies exhibited decrease in optical band gap with increase in Cu-to-S molar ratio. Electrical properties revealed that as-synthesized CuS films have low sheet resistance (1.47–2.45 Ω/□), high carrier mobility (8.90–54.89 cm^2/Vs) and excellent sheet concentration (10^{16}–10^{18}/cm^2). Photovoltaics characteristics of DSSC incorporating optimized CuS as counter electrode showed power conversion efficiency of ~1.05% with V_{oc} ~ 0.46 V, I_{sc} ~ 1.01 mA/cm^2 and fill factor ~0.34%. Further optimization is needed for improving the photovoltaic performance of DSSCs.

Acknowledgements The authors are thankful to the Department of Science and Technology (DST) and Ministry of New and Renewable Energy (MNRE), Government of India and Centre for Nanomaterials and Quantum Systems (CNQS), Savitribai Phule Pune University, Pune for the financial support. Sachin Rondiya is also grateful to the Dr. Babasaheb Ambedkar Research and Training Institute, Pune for the research fellowship and financial assistance. One of the authors Sandesh Jadkar is thankful to University Grants Commission, New Delhi for special financial support under UPE program.

References

1. P.K. Nair, M.T.S. Nair, J. Phys. D **24/1**, 83 (1991)
2. R.J. Goble, Can. Mineral **23**, 61 (1985)
3. J. Johansson, J. Kostamo, M. Karppinen, L. Niinisto, J. Mater. Chem. **12**, 1022 (2002)
4. V.I. Klimov, P. Haring-Bolivar, V.A. Karavanskii, Superlattices Microstruct. **20**, 395 (1996)
5. V.N. Konev, V.N. Chebotin, S.A. Fomenkov, Inorg. Mater. **21**, 205 (1985)

6. I.I. Mazin, Phys. Rev. B **85**, 115133 (2012)
7. P.K. Nair, M.T.S. Nair, Semicond. Sci. Technol. **4**, 191 (1989)
8. S. Lindroos, A. Arnold, M. Leskel, Appl. Surf. Sci. **158**, 75 (2000)
9. G. Liu, T. Schulmeyer, J. Brötz, A. Klein, W. Jaegermann, Thin Solid Films **431–432**, 477 (2003)
10. J.S. Chung, H.J. Sohn, J. Power Sources **108**, 226 (2002)
11. R.S. Mane, C.D. Lokhande, Mater. Chem. Phys. **65**, 1 (2000)
12. Q. Wang, N. An, Y. Bai, H. Hang, J. Li, X. Lu, Y. Liu, F. Wang, Z. Li, Z. Lei, Int. J. Hydr. Energy **38**, 10739 (2013)
13. T. Sakamoto, H. Sunamura, H. Kawaura, T. Hasegawa, T. Nakayama, M. Aonob, Appl. Phys. Lett. **82**, 3032 (2003)
14. Y. Han, Y. Wang, W. Gao, Y. Wang, L. Jiao, H. Yuan, S. Liu, Powder Technol. **212**, 64 (2011)
15. A. Setkus, A. Galdikas, A. Mironas, A. Mironas, I. Simkiene, I. Ancutiene, V. Janickis, S. Kaciulis, G. Mattogno, M. Ingo, Thin Solid Films **391**, 275 (2001)
16. S.W. Hsu, W. Bryks, A.R. Tao, Chem. Mater. **4**, 3765 (2012)
17. W. Ke, G. Fang, H. Lei, P. Qin, H. Tao, W. Zeng, J. Wang, X. Zhao, J. Power Sources **248**, 809 (2014)
18. P. Kar, S. Farsinezhad, X. Zhang, K. Shankar, Nanoscale **6**, 14305 (2014)
19. H. Rao, W. Sun, S. Ye, W. Yan, Y. Li, H. Peng, Z. Liu, Z. Bian, C. Huang, ACS Appl. Mater. Interfaces **8**, 7800 (2016)
20. M. Al-Shakban, P.D. Matthews, G. Deogratias, P.D. McNaughter, J. Raftery, I. Yrezabal, E.B. Mubofu, P. O'Brien, Inorg. Chem. **56**, 9247 (2017)
21. W. Du, L. Liao, L. Yang, A. Qin, A. Liang, Sci. Rep. **7**, 11451 (2017)
22. Y. Zhai, M. Shim, Chem. Mater. **29**, 2390 (2017)
23. F. Ghribi, A. Alyamani, Z. Ben Ayadi, K. Djessas, L. Mir, Energy Proc. **84**, 197 (2015)
24. H. Mazor, D. Golodnitsky, L. Burstein, E. Peled, Solid-State Lett. **12**, A232 (2009)
25. A. Bollero, M. Grossberg, B. Asenjo, M.T. Gutiérrez, Surf. Coat. Technol. **204**, 593 (2009)
26. S.K. Maji, N. Mukherjee, A.K. Dutta, D.N. Srivastava, P. Paul, B. Karmakar, A. Mondal, B. Adhikary, Mater. Chem. Phys. **130**, 392 (2011)
27. M.T.S. Nair, L. Guerrero, P.K. Nair, Semicond. Sci. Technol. **13**, 1164 (1998)
28. L. Reijnen, B. Meester, F. Lange, J. Schoonman, A. Goossens, Chem. Mater. **17**, 2724 (2005)
29. S.H. Chaki, M.P. Deshpande, J.P. Tailor, Thin Solid Films **550**, 291 (2014)
30. Y. Lei, H. Jia, Z. Zheng, Y. Gao, X. Chen, H. Hou, Cryst. Eng. Commun. **13**, 6212 (2011)
31. A.A. Iribe, M.C. Enríquez, D.B. Mendoza, T.M. Reynoso, E.L. Rodríguez, R.R. Bon, S.J. Castillo, Chalcogenide Lett. **10**, 543 (2013)
32. H. Chen, L. Zhu, H. Liu, W. Li, J. Phys. Chem. C **117**, 3739 (2013)
33. B. Guzeldir, M. Saglam, A. Ates, Acta Phys. Pol. A **121**, 33 (2012)
34. A. Sana Riyaz, A. Parveen, Azam, Perspect. Sci. **8**, 632 (2016)
35. M. Adelifard, H. Eshghi, M.M.B. Mohagheghi, Appl. Surf. Sci. **258**, 5733 (2012)
36. F.A. Sabah, N. Ahmed, Z. Hassan, J. Electron. Mater. **46**, 218 (2017)
37. P.V. Nho, P.H. Ngan, N.Q. Tien, H.D. Viet, Chalcogenide Lett. **9/10**, 397 (2012)
38. M.B. Rajendra Prasad, P.S. Tamboli, R.V. Ingle, K.D. Diwate, P.K. Baviskar, B.R. Sankpal, K.C. Mohite, S.R. Jadkar, H.M. Pathan, Curr. Appl. Phys. **17**, 1691 (2017)
39. M. Saranya, C. Santhosh, R. Ramachandran, A. Nirmala Grace, J. Nanotechnol. 8 (2014)
40. B. Cullity, S. Stock, *Elements of X-ray Diffraction*, 3rd edn. (Princeton Hall, Upper Saddle River, 2001)
41. N. Yeryukov, A. Milekhin, L. Sveshnikov, T. Duda, L. Pokrovsky, A. Gutakovskii, S. Batsanov, E. Rodyakina, A. Latyshev, D. Zahn, J. Phys. Chem. C **118**, 23409 (2014)
42. Z. Zhan, C. Liu, L. Zheng, G. Sun, B. Li, Q. Zhang, Phys. Chem. Chem. Phys. **913**, 20471 (2011)
43. A.G. Milekhin, N.A. Yeryukov, L.L. Sveshnikova, T.A. Duda, E.E. Rodyakina, V.A. Gridchin, E.S. Sheremet, D.R.T. Zahn, Beilstein J. Nanotechnol. **6**, 749 (2015)
44. L. Chen, W. Yu, Y. Li, Powder Technol. **191**, 52 (2009)
45. H.L. Xu, W.Z. Wang, W. Zhu, L. Zhou, Nanotechnology **17**, 3649 (2006)
46. A. Vasuhi, R.J. Xavier, R. Chandramohan, S. Muthukumaran, K. Dhanabalan, M. Ashokkumar, P. Parameswaran, J. Mater. Sci. Mater. Electron. **25**, 824 (2014)
47. J. Tauc, *Amorphous and Liquid Semiconductors*. (Springer, New York, 2012)
48. Y. Huang, H. Xiao, S. Chen, C. Wang, Ceram. Inter. **35**, 905 (2009)
49. C.M. Donega, Chem. Soc. Rev. **40**, 1512 (2011)
50. K.D. Yuan, J.J. Wu, M.L. Liu, L.L. Zhang, F.F. Xu, L.D. Chen, F.Q. Huang, Appl. Phys. Lett. **93**, 132106 (2008)
51. H. Morkoc, *Handbook of Nitride Semiconductors and Devices, Materials Properties, Physics and Growth*, vol. 1. (Wiley, Hoboken, 2009)
52. Q. Shen, A. Yamada, S. Tamura, T. Toyoda, J. Appl. Phys. Lett. **97**, 123107 (2010)
53. K. Tezuka, W.C. Sheets, R. Kurihara, Y.J. Shan, H. Imoto, T.J. Marks, K.R. Poeppelmeier, Solid State Sci. **9**, 95 (2007)
54. C.Justin Raj, K. Prabakar, A.D. Savariraj, H.J. Kim, Electrochim. Acta **103**, 231 (2013)
55. B. Luo, Y. Deng, Y. Wang, Z. Zhang, M. Tan, J. Alloys Compd. **517**, 192 (2012)
56. H. Feng, L. Chen, L. Yuan, Q. Cai, Chem. Eng. J. **215**, 591 (2013)
57. Z. Yang, C.Y. Chen, C.W. Liu, C.L. Li, H.T. Chang, Adv. Energy Mater. **1**, 259 (2011)